Volume 2
Number 1
January 2023
Pages 1–228

Energy Advances

rsc.li/energy-advances

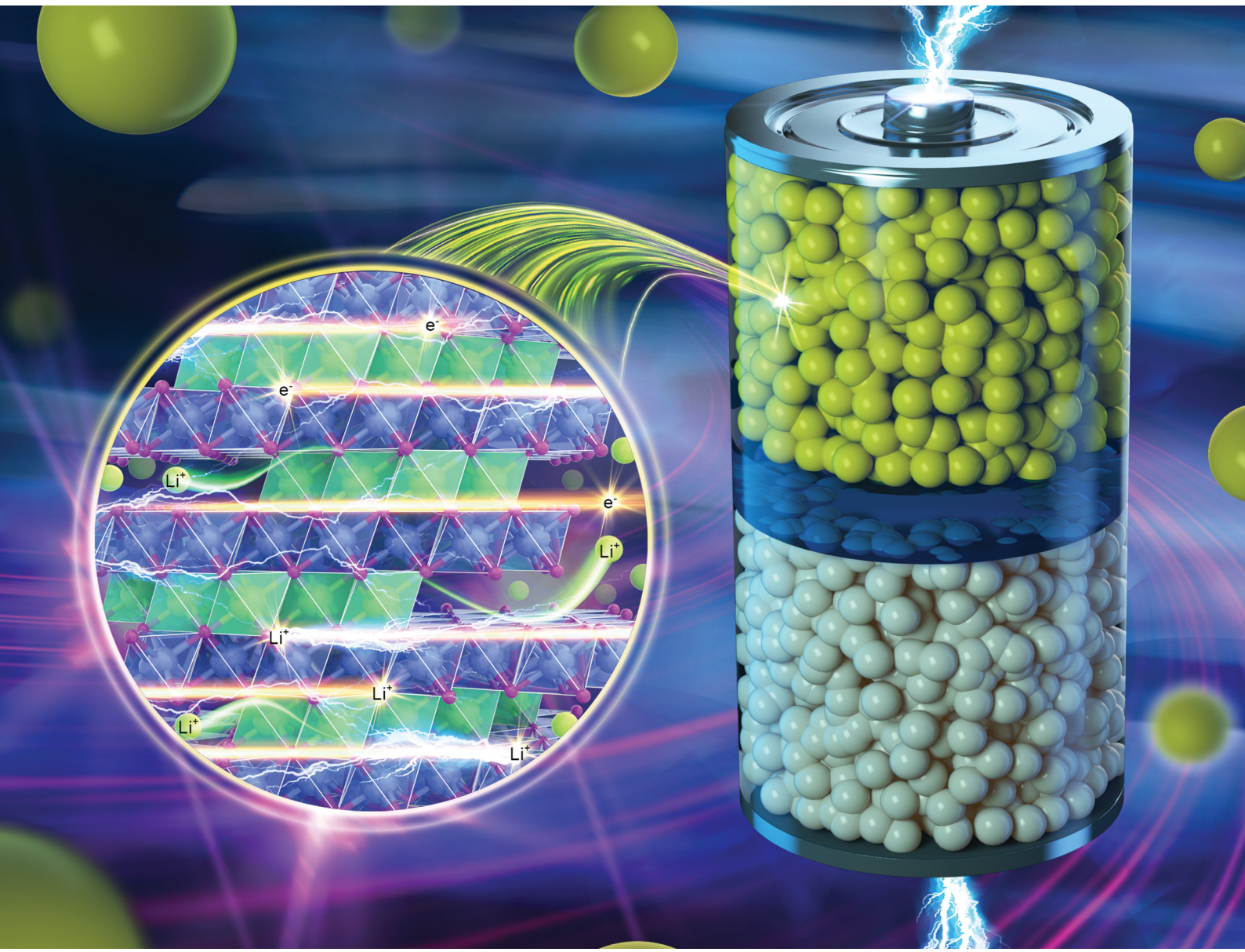

ISSN 2753-1457

ROYAL SOCIETY OF CHEMISTRY

PAPER
Li Wang, Jonghyun Park, Xiangming He *et al.*
Atomic-scale insight into the lattice volume plunge of Li_xCoO_2 upon deep delithiation

Energy Advances

ROYAL SOCIETY OF CHEMISTRY

PAPER

View Article Online
View Journal | View Issue

Cite this: *Energy Adv.*, 2023, 2, 103

Atomic-scale insight into the lattice volume plunge of Li_xCoO_2 upon deep delithiation†

Yufang He,[a] Li Wang,*[a] Bo Zhang,[a] Hiep Pham,[b] Hong Xu,[a] Jonghyun Park*[b] and Xiangming He*[a]

The practical capacity utilization of $LiCoO_2$ is limited to 50–70% due to the dramatic volume shrinkage induced cracks and subsequent interface parasitic reactions at high voltage. However, the fundamental understanding of the dramatic lattice volume shrinkage remains unclear. In this work, we discover that the delithiation paths have an impact on the lattice volume turning point of Li_xCoO_2, where the corresponding capacity utilization can be as low as 62.5% or as high as 75% consequently. In addition, the O ↔ O interlayer distance across the Li layer ($O_{(d3)}$) mainly contributes to the volume increase before 62.5–75% delithiation, and the O ↔ O interlayer distance across the Co layer ($O_{(d2)}$) is the dominant factor for the dramatic volume decrease after the volume turning point. The electron localization function (ELF) around O keeps increasing during delithiation and it increases significantly after more than 62.5% delithiation, indicating that the lattice oxygen participates in charge compensation during the whole delithiation process and it becomes the main contributor to the charge compensation at a high delithiated state compared with Co. This work unravels the fundamental reason for the dramatic volume shrinkage of Li_xCoO_2 at high voltage. It claims that the antisite defects (Co_{Li}) of $LiCoO_2$ should be designed carefully owing to the weaker Co–O bond strength and further oxygen release, which accelerate the degradation of $LiCoO_2$, although it can increase the voltage of $LiCoO_2$. More importantly, $LiCoO_2$ material design with elemental doping, oxygen defects (V_O), Li defects (V_{Li}), and Co defects (V_{Co}) will contribute to the capacity utilization of $LiCoO_2$.

Received 12th October 2022,
Accepted 1st November 2022

DOI: 10.1039/d2ya00278g

rsc.li/energy-advances

Introduction

$LiCoO_2$ was the first commercialized cathode material for lithium-ion batteries (LIBs) by the Sony Corporation in 1991 and it remains one of the most heavily used cathodes for consumer electronics owing to its high tap density, high initial coulombic efficiency, and high volumetric energy density.[1–5] For a long time, only about half of the Li was utilized in the $LiCoO_2$ cathode material. Researchers try to achieve more capacity while maintaining the stability of the $LiCoO_2$ cathode material to fully utilize the energy density, such as doping and coating, which enables reversible Li-utilization up to 0.7 at high voltage,[4] and little or no oxygen release from the bulk.[6] However, deeper delithiation would lead to oxygen release or particle breakage, leading to capacity fading because of prominent parasitic reactions at the Li_xCoO_2/electrolyte interface and material loss.[4,7–9] These indicate that keeping the particle integrity during deep lithiation is important to achieve $LiCoO_2$ with high capacity.

Previous studies showed that the lattice volume of $LiCoO_2$ experiences a dramatic decrease at high voltage and the volume turning points differ depending on different $LiCoO_2$ samples.[4,9–13] The existence of the sample difference results in the variation of capacity utilization of $LiCoO_2$. The reported dramatic volume turning point of Li_xCoO_2 ranges between 50% and 70% delithiation rates. Dahn *et al.* reported that the volume of $LiCoO_2$ decreases around 4.2 V and the corresponding Li utilization is around 50%.[12] Besides, the volume change of $LiCoO_2$ is thought to be dominated by lattice *c*, and Tarascon *et al.* proposed that the lattice *c* parameter stably increased owing to the increasing electrostatic repulsion of O ↔ O interactions of adjacent CoO_6 layers during delithiation. Then, the *c* parameter underwent a dramatic decrease when the delithiation ratio was 54%, stemming from a transformation from monoclinic distortion to a hexagonal structure.[10,14] Van der Ven *et al.* also demonstrated that the lattice *c* parameter increases and then decreases dramatically when delithiation was over 60% Li.[11] Liu *et al.* claimed that the reversible Li utilization of La- and Al-co-doped $LiCoO_2$ was

[a] *Institute of Nuclear and New Energy Technology, Tsinghua University, Beijing 100084, China. E-mail: wang-l@tsinghua.edu.cn, hexm@tsinghua.edu.cn*
[b] *Department of Mechanical Engineering and Aerospace Engineering, Missouri University of Science and Technology, Rolla, 65401, USA. E-mail: parkjonghy@mst.edu*

† Electronic supplementary information (ESI) available. See DOI: https://doi.org/10.1039/d2ya00278g

increased to 70% with the cut-off voltage increasing to 4.5 V.[4] Barker *et al.* showed that the Li utilization in $LiCoO_2$ reached up to 64% with 100% coulombic efficiency.[13] It is well accepted that the dramatic volume change of Li_xCoO_2 at high voltage is closely related to the O ↔ O interaction environments in $LiCoO_2$, including O ↔ O interaction environments in the CoO_6 layer and O ↔ O interaction environment across the Li layer. Recently, the oxygen redox reaction is regarded as the predominant factor for the electrochemical performance of transition metal oxide cathodes at high voltage,[15–20] where O contributes much more to charge compensation than Co.[6] The oxygen redox reaction at high voltage has an impact on the volume change of Li_xCoO_2. However, there is no clear understanding of the variation of the dramatic volume turning point of Li_xCoO_2 at high voltage, as well as the explicit perception regarding the change of O ↔ O interaction environment.

In this work, the fundamental reasons for the lattice volume shrinkage of $LiCoO_2$ during delithiation are investigated *via* theoretical calculations, especially at high voltage. We found that there exists a relationship between delithiation paths and the lattice volume plunging point during charging, which determines the reversible capabilities of the $LiCoO_2$ cathode. Four different random delithiation paths are considered. The O ↔ O distances with three different O ↔ O interaction environments in Li_xCoO_2 along delithiation path 1 are further investigated, which are O ↔ O intralayer distance ($O_{(d1)}$), O ↔ O interlayer distance across the Co layer ($O_{(d2)}$), and O ↔ O interlayer distance across the Li layer ($O_{(d3)}$). To further identify the electronic properties, the electron localization function (ELF) of Li_xCoO_2 is calculated. There is peroxo-like O–O formation during delithiation. The analysis of the total density of states (TDOS) of Li_xCoO_2 and the projected density of states (PDOS) of O and Co uncovers that the oxygen oxidation and the dramatic volume shrinkage point of Li_xCoO_2 are correlated. In addition, the phase transition of Li_xCoO_2 is examined for the reliability of these simulation results. This work provides theoretical guidance for reasonable materials design and synthesis to achieve a higher capacity utilization of $LiCoO_2$ cathode.

Methods

The lattice volume plunge of Li_xCoO_2 during delithiation is crucial for the energy density of LIBs. To study the fundamental reason for the lattice volume shrinkage of Li_xCoO_2 during delithiation, density functional theory (DFT) calculations are performed by using the Vienna *Ab initio* Simulation Package (VASP) code.[21] The Perdew–Burke–Ernzerhof (PBE) functional is employed to approximate the exchange–correlation function. The projector augmented wave (PAW) method[22–24] is used for electron and core interactions. A Hubbard U parameter of 4.91 eV is applied to the delocalization correction of the Co d-orbital.[25] The cutoff energy is set at 520 eV. The convergence criterion in the electronic self-consistent iteration is 10^{-4} eV and the convergence criterion for ionic relaxation is set at 0.03 eV $Å^{-1}$. The layered $LiCoO_2$ (space group: $R3m$) structure is used for calculations, which consists of 48 Li, 48 Co, and 96 O. The cell volume is allowed to change[26] and the delithiated Li_xCoO_2 structure is fully relaxed during structure optimization. The volume calculation of Li_xCoO_2 is performed by considering four different delithiation paths. The electron localization function (ELF) of Li_xCoO_2 at different delithiation states is examined[27] to further study the valence states and bonding states of Co and O. The ELF and the phase transformation of Li_xCoO_2 is visualized with the aid of VESTA software.[28] The density of states (DOS)[29] of Li_xCoO_2 is examined *via* executing the 'split_dos' script from the VASP output. Besides, the Bader charge analysis[30–33] is performed to calculate the charge states of Co and O in Li_xCoO_2 during the delithiation process. In addition, the volume change of the Li_xCoO_2 cathode during delithiation is characterized using *in situ* X-ray diffraction (XRD).[34]

Results and discussion

To reveal the fundamental reason for the volume change of Li_xCoO_2 during Li extraction, the lattice volumes of Li_xCoO_2 at

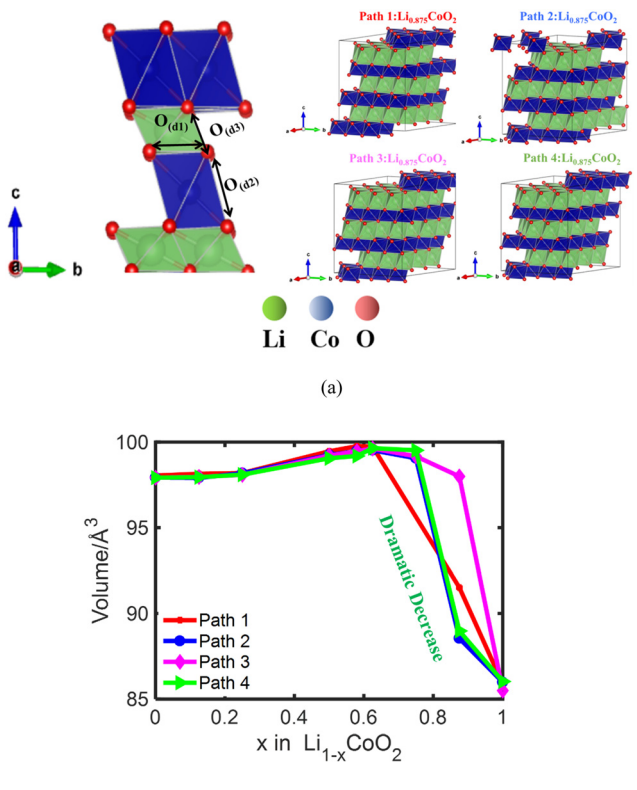

Fig. 1 (a) The three different O ↔ O interactions including the O ↔ O distances $O_{(d1)}$, $O_{(d2)}$ and $O_{(d3)}$, and schematic of four different random delithiation paths in Li_xCoO_2 considered during volume calculations using DFT; (b) the volume change of Li_xCoO_2 along four different random delithiation paths. It demonstrates that the volume of Li_xCoO_2 stably increases and then decreases dramatically when 62.5–75% Li is removed from the host, which has the same tendency as the volume change of Li_xCoO_2 measured with the XRD experiment.

different delithiation states are first calculated. The layered $LiCoO_2$ structure with the *R3m* space group used for density functional theory (DFT) calculations is shown in Fig. 1(a) and Fig. S1a (ESI†). Fig. 1(a) also demonstrates that the lattice volume of $LiCoO_2$ is closely related to the intralayer O ↔ O distance $O_{(d1)}$, the O ↔ O interlayer distance across the Co layer $O_{(d2)}$, and the O ↔ O interlayer distance across the Li layer $O_{(d3)}$. As shown in Fig. 1(b), the volume of Li_xCoO_2 with four different delithiation paths stably increases and then decreases dramatically when 62.5–75% Li is removed from the host, which has the same trend as the volume change of Li_xCoO_2 measured with the *in situ* XRD experiment (Fig. S1b, ESI†). The simulation results are different from the experimental results because the simulation results are based on an ideal model, assuming that the $LiCoO_2$ particles are uniform and pure single crystals. However, in reality, it is challenging to reach the theoretical value. In addition, the practical $LiCoO_2$ particles in experiments possess different kinds of defects. There are four types of defects in $LiCoO_2$, including antisite cation (Co_{Li}), Li-ion vacancy (V_{Li}), Co-ion vacancy (V_{Co}), and O-ion vacancy (V_O).[35] The antisite defects and V_O defects lead to an increase in intercalation potential. A higher intercalation potential of $LiCoO_2$ *versus* Li/Li^+ indicates a higher discharge voltage.[36] Meanwhile, the $LiCoO_2$ with antisite defects (Co_{Li}) contributes to weaker Co–O bond strength and further oxygen release,[37,38] which might be responsible for the variation of the dramatic volume change point of $LiCoO_2$. Whilst the V_{Li} and V_{Co} defects are responsible for the electron conductivity and charge compensation during delithiation. It is also reported that oxygen defects can ensure a high degree of oxygen redox.[39] Furthermore, it is claimed that the phase transitions and volume variation are very sensitive to the impurity levels of $LiCoO_2$ particles and it can be used as a quality check for the synthetic $LiCoO_2$ material.[13,40] Fig. S1c (ESI†) shows that the lattice *c* parameter of Li_xCoO_2 increases with delithiation and then decreases after more than 62.5–75% delithiation, which shows the same trend as the volume change of Li_xCoO_2. Meanwhile, the lattice *a* parameter of Li_xCoO_2 decreases and then

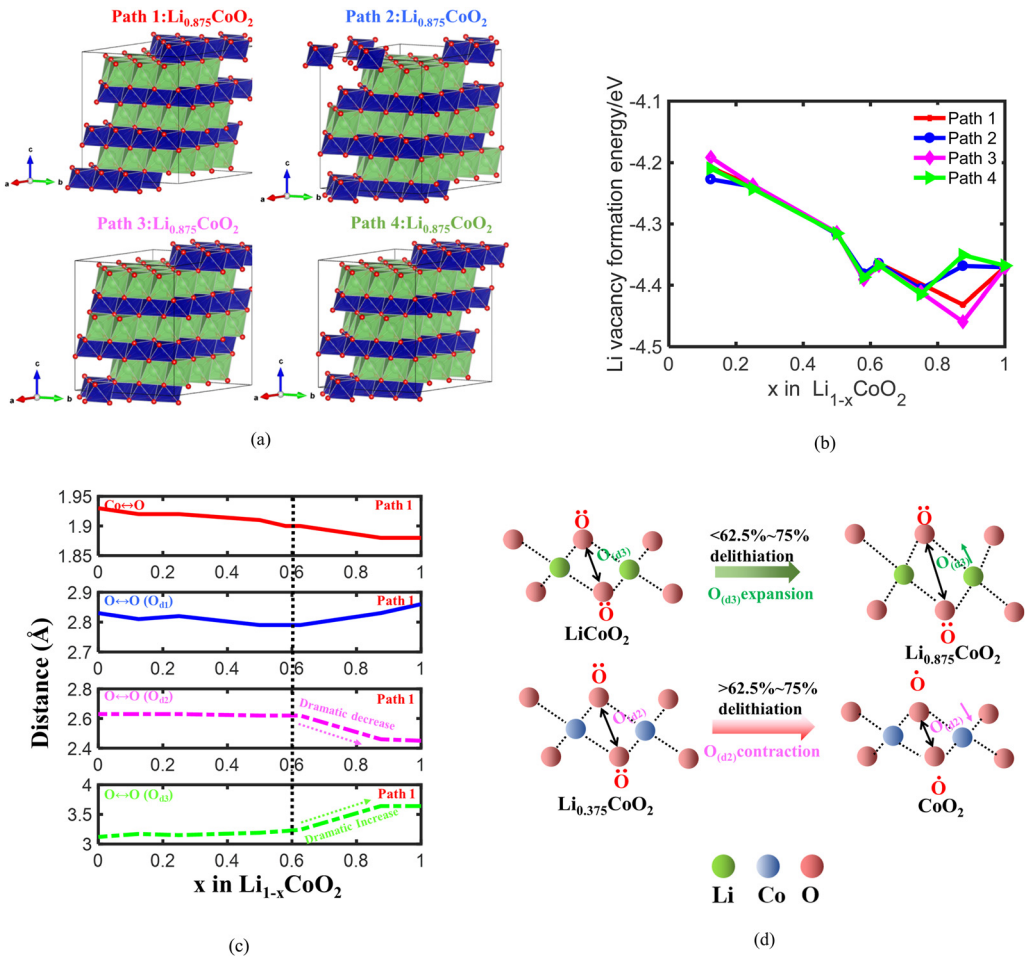

Fig. 2 The Li_xCoO_2 structure during initial delithiation with four different delithiation paths (a); the Li vacancy formation energy of Li_xCoO_2 along four different delithiation paths (b); the Co ↔ O distance, the O ↔ O intralayer distance $O_{(d1)}$, the O ↔ O interlayer distance across the Co layer $O_{(d2)}$, and the O ↔ O interlayer distance across the Li layer $O_{(d3)}$ along delithiation path 1 (c); the schematic illustrating the mechanism of O ↔ O interaction induced volume change at different delithiation states. The O ↔ O interlayer distance across the Li layer $O_{(d3)}$ mainly contributes to the increasing volume of Li_xCoO_2 when delithiation is less than 62.5% due to the electrostatic repulsion interaction between negatively charged O (d).

increases after more than 62.5–75% removal of Li (Fig. S1d, ESI†), which is consistent with reported experimental results.[41] It also shows that the volume change of Li_xCoO_2 is influenced by the lattice *c* parameter of Li_xCoO_2, which is consistent with reported work.[11] More importantly, it is reported that the ordering of lithium and vacancy has a profound effect on the electrochemical performance of Li-ion batteries.[42] The lattice volume of Li_xCoO_2 shrinks at different delithiation capacities by considering four different delithiation paths. Fig. 1(b) clearly shows that different delithiation paths in Li_xCoO_2 produce different volume turning points, where it is between 62.5% and 75%, explaining why there exists a dramatic volume turning point difference between different experimental works. The difference in delithiation paths during the charging process may come from material defects and synthesis process of $LiCoO_2$. To improve the delithiation performance of $LiCoO_2$, the antisite defects of $LiCoO_2$ should be designed carefully because although it contributes to the increase of the voltage of $LiCoO_2$, it will cause a weaker Co–O bond strength and further oxygen release as well. More crucially, $LiCoO_2$ material design with V_O, V_{Li} and V_{Co} will contribute to the improvement of voltage, electron conductivity, and charge compensation during the delithiation process.

To further identify the fundamental reason for the volume changes of Li_xCoO_2, one of the four delithiation paths is chosen to analyze the change of O ↔ O interactions and the Co ↔ O interaction during delithiation. The initial delithiation structure of Li_xCoO_2 along four different delithiation paths is shown in Fig. 2(a) and the Li vacancy formation energy of the four different delithiation paths is demonstrated in Fig. 2(b). The Li formation energy can measure how easily for Li to be extracted from the host, where a lower Li formation energy indicates the easier formation of Li vacancy. It shows that Li prefers to be extracted from the host during the whole delithiation owing to the negative value of Li vacancy formation energy. Besides, the Li vacancy formation energy of the four delithiation paths is almost the same when delithiation is less than 75%, except that there is a small difference when 12.5% Li is extracted. The Li vacancy formation energy of path 3 becomes the lowest and that of path 4 becomes the highest when delithiation is more than 75%. Based on the Li vacancy formation energy of the four delithiation paths, path 1 is selected for further analysis because the Li vacancy formation energy values of path 1 are located in the middle of the four paths during delithiation process. Fig. 2(c) shows that the Co ↔ O distance keeps decreasing from 1.93 Å to 1.88 Å, coinciding with the increasing charge state of Co attributed to the charge compensation delithiation. Besides, the O ↔ O intralayer distance $O_{(d1)}$ decreases slightly from 2.83 Å to 2.79 Å before delithiation reaching 62.5% and then increases rapidly to 2.86 Å between

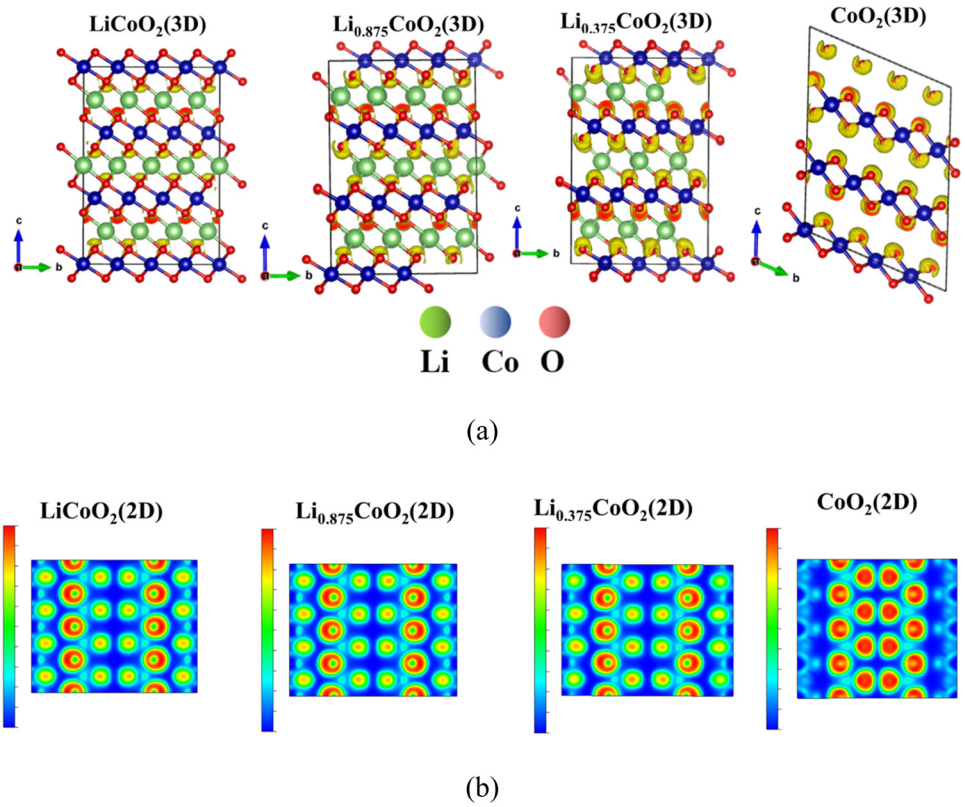

Fig. 3 The 3D (a) and 2D (b) electron localization function of Li_xCoO_2 during delithiation (the red color means electron localization, indicating the existence of lone pair electrons, while the blue color means electron delocalization showing that there is a bonding state). The electrons localized around O increase during delithiation and the ELF increases dramatically after delithiation is more than 62.5%, implying that O oxidation occurs and the lattice oxygen mainly contributes to the charge compensation at a high delithiation state.

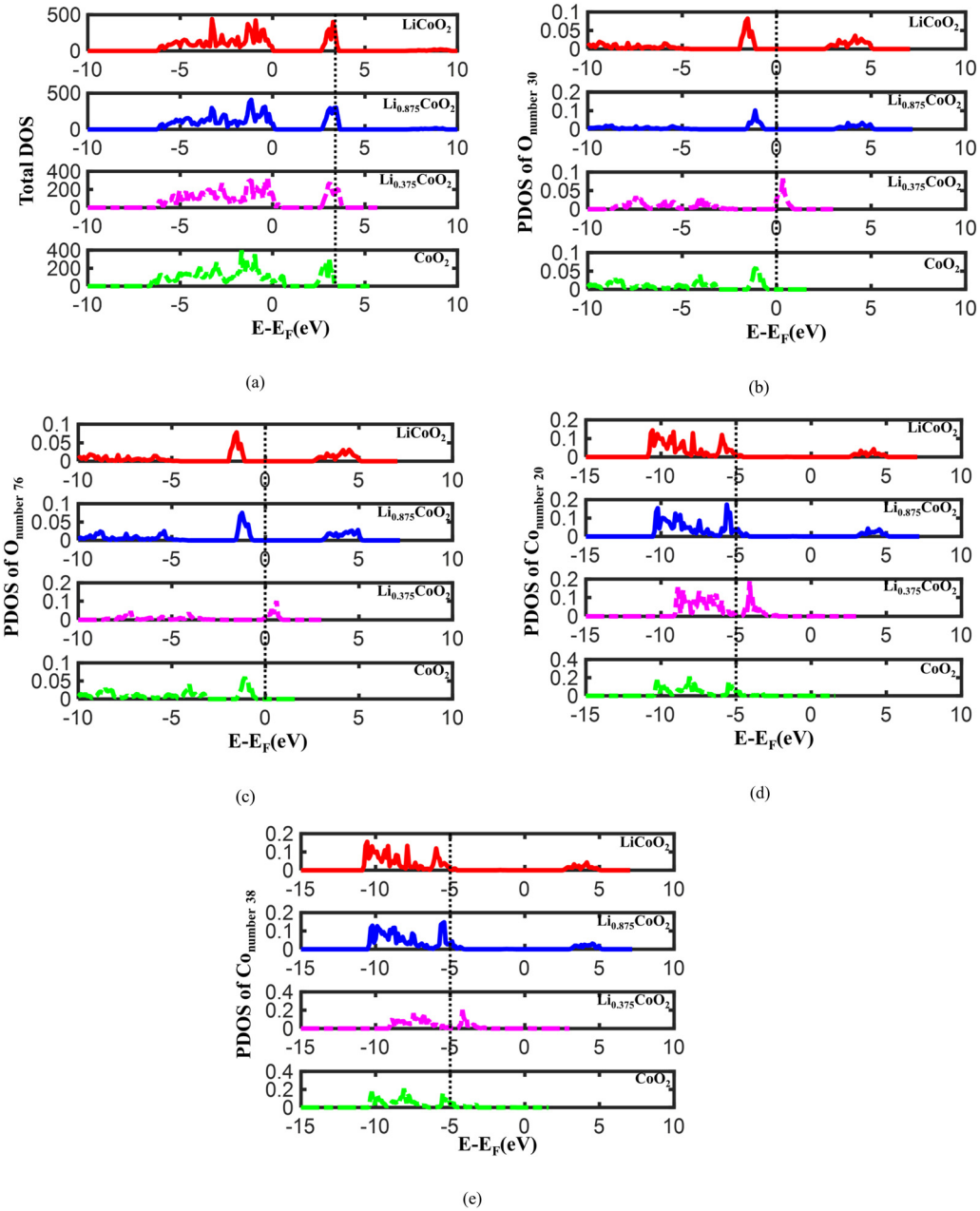

Fig. 4 The TDOS of Li_xCoO_2 during delithiation (a), the PDOS of $O_{number\ 30}$ with surrounded Li extracted (b), the PDOS of $O_{number\ 76}$ without surrounded Li extracted (c), and the PDOS of $Co_{number\ 20}$ (d) and $Co_{number\ 38}$ (e) during delithiation. The energy level of the PDOS peak of O keeps increasing until 62.5% Li is extracted from Li_xCoO_2, implying that it becomes easier for O oxidation to occur with increasing delithiation, while the energy level of the PDOS peak shifts to a lower energy level when delithiation is more than 62.5%, indicating that there is a correlation between O oxidation and the dramatic volume change of Li_xCoO_2.

62.5% and 100% delithiation (Fig. 2(c)). Meanwhile, the O ↔ O distance across the Co layer $O_{(d2)}$ is almost unchanged until 37.5% delithiation and the O ↔ O distance across the Co layer $O_{(d2)}$ decreases dramatically from 2.62 Å to 2.46 Å after the delithiation is more than 62.5%. In contrast, the O ↔ O interlayer distance across the Li layer $O_{(d3)}$ increases slightly and then increases dramatically after 62.5% Li is removed (Fig. 2(c)). The lowest O ↔ O distance is around 2.46 Å, which is almost the same as the reported results.[6] The O ↔ O interlayer distance across the Co layer and Li layer dominates the volume change of $LiCoO_2$ during delithiation. The O ↔ O interlayer distance across the Li layer $O_{(d3)}$ dominates the volume change of Li_xCoO_2 when delithiation is less than 62.5% due to the electrostatic repulsion interaction between negatively charged O (Fig. 2(d)). More importantly, the O ↔ O interlayer distance across the Co layer $O_{(d2)}$ is mainly

responsible for the dramatic volume turning point of Li_xCoO_2 when delithiation is more than 62.5% owing to the oxygen oxidation at high voltage.

To further investigate the electronic structure of the three O ↔ O interaction environments that induced the dramatic volume change of Li_xCoO_2, the electron localization function (ELF) of Li_xCoO_2 is calculated.[43] The ELF results show the bonding type and lone pair electrons of Li_xCoO_2, where the red color means fully localized and the blue color represents fully delocalized electrons. The fully localized electrons indicate the existence of a lone-pair electron, while the delocalized electrons imply the bonding state. Fig. 3(a) and Fig. S2a (ESI†) illustrate that the ELF around O keeps increasing during delithiation, implying that there exist more lone-pair electrons and the valence state of oxygen gradually changes from O^{2-} to $(O_2)^{n-}$ $(1 \leq n \leq 3)$, which indicates that the oxygen contributes to the charge compensation and there is O–O bond formation during the delithiation process. But Yang *et al.* claimed that there is no O–O bond formation *via* COOP analysis.[6] We believe the ELF calculation is more comprehensive and reasonable because the electron localization function is calculated by considering the entire Li_xCoO_2, whereas the COOP analysis is conducted only checking a specific O–O bonding state in Li_xCoO_2, which is not sufficient to represent the whole Li_xCoO_2 structure during delithiation. The 2D electron localization function of Li_xCoO_2 shown in Fig. 3(b) and Fig. S2b (ESI†) is sliced with half of lattice *b* and the Miller index is (010), and it clearly shows that the ELF around O increases significantly after more than 62.5% delithiation. Therefore, the lattice oxygen in Li_xCoO_2 participates in charge compensation during the whole delithiation process and it becomes the main contributor to the charge compensation at a highly delithiated state compared with Co, where the oxygen redox reaction occurs.

To further reveal the electronic properties of Li_xCoO_2 during delithiation, the total density of states (TDOS) and the projected density of states (PDOS) of O and Co in Li_xCoO_2 are calculated. Fig. 4(a) and Fig. S3a (ESI†) display that the highest energy peak of TDOS shifts to a lower energy level during delithiation. The lower energy state of TDOS suggests that the electrons in an atomic orbital are more difficult to escape. Therefore, it becomes harder for Li and electrons to escape from the Li_xCoO_2 host during delithiation, which is reasonable due to the limited reversibility of $LiCoO_2$ cathode materials. Then, the electronic properties of O in Li_xCoO_2 are analyzed and the lattice oxygen atoms with and without surrounded Li extracted are considered. The $O_{number\,30}$ and $O_{number\,76}$ are in the oxygen sites with and without surrounded Li extracted respectively. The atomic environments of $O_{number\,30}$ and $O_{number\,76}$ are shown in Fig. S3b (ESI†). As illustrated in Fig. 4(b) and Fig. S3c (ESI†), the energy level of the PDOS peak of $O_{number\,30}$ initially increases and then decreases when delithiation is around 62.5%, which indicates that oxygen oxidation occurs more easily when delithiation increases to 62.5%. However, after the dramatic volume change turning point, the energy level of the PDOS peak decreases, implying that it becomes more difficult for oxygen oxidation to occur when the dramatic volume change of Li_xCoO_2 starts. It

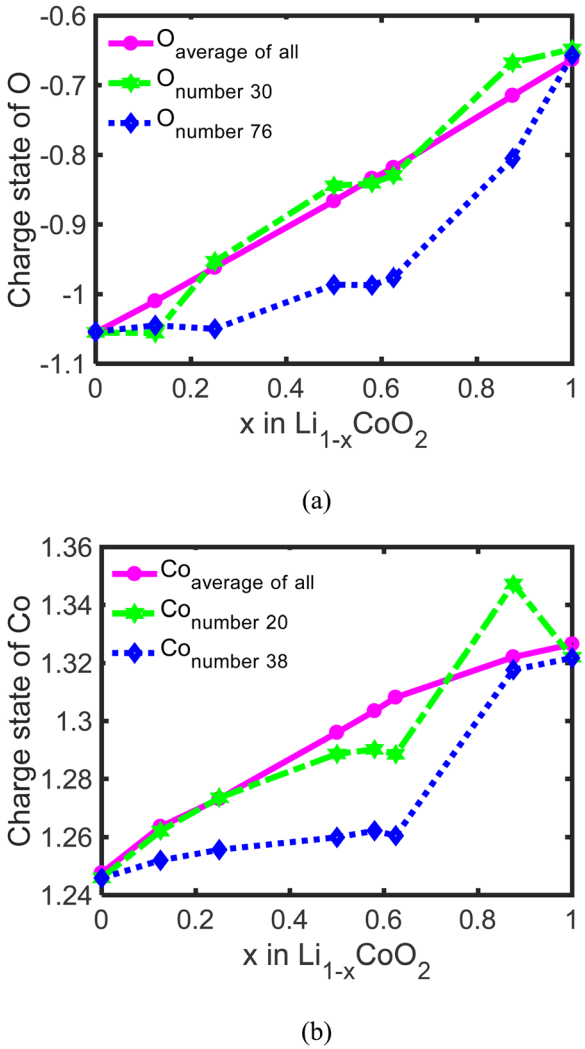

Fig. 5 The average charge states of all O, individual $O_{number\,30}$ with surrounded Li extracted, and individual $O_{number\,76}$ without surrounded Li extracted in Li_xCoO_2 during delithiation (a); the average charge states of all Co, individual $Co_{number\,20}$, and individual $Co_{number\,38}$ in Li_xCoO_2 during delithiation (b).

agrees well with the volume change and the O ↔ O distance calculation. It further provides the fundamental reason for the dramatic volume change occurring after more than 62.5% delithiation, corresponding to the reported experimental results that the reversible capacity of Li_xCoO_2 is around 50–70%.[12,13] Therefore, the oxygen oxidation and the dramatic volume change point of Li_xCoO_2 are correlated. The energy level of the PDOS peak of $O_{number\,76}$ also increases and then decreases, demonstrating that the oxygen oxidation capability is influenced by the whole delithiation state instead of the local atomic environment (Fig. 4(c) and Fig. S3d, ESI†). In addition, the PDOS of Co is checked and the atomic environments of $Co_{number\,20}$ and $Co_{number\,38}$ are demonstrated in Fig. S3b (ESI†). As shown in Fig. 4(d) and Fig. S3e (ESI†), the energy level of the PDOS peak of $Co_{number\,20}$ increases with delithiation and then decreases because the dramatic volume change of Li_xCoO_2

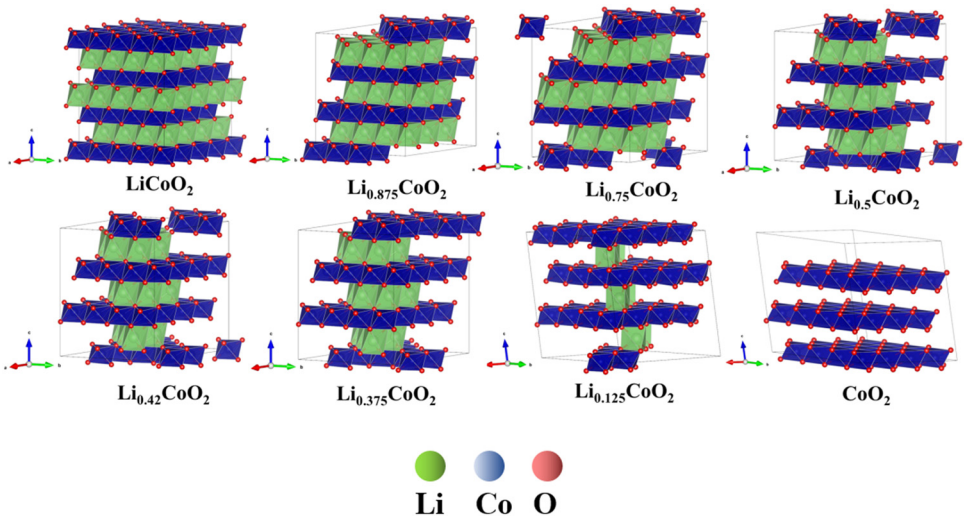

Fig. 6 The phase transformation of Li_xCoO_2 during delithiation: the Li_xCoO_2 evolves from the O3 phase to the O1 phase and the gradual angle keeps decreasing during delithiation.[48]

starts. The energy level of the PDOS of $Co_{number\,38}$ shows the same trend as $Co_{number\,20}$ (Fig. 4(e) and Fig. S3f, ESI†), which suggests that the Co oxidation is also mainly related to the whole delithiation state of Li_xCoO_2 instead of the local atomic environment.

To uncover the effect of oxygen charge compensation for delithiation on the dramatic volume change of Li_xCoO_2, the average charge states of all O and Co, and the charge states of $O_{number\,30}$, $O_{number\,76}$, $Co_{number\,20}$, and $Co_{number\,38}$ are calculated *via* Bader analysis.[30–33] The average charge state of O increases from −1.05 to −0.67 (Fig. 5(a)) and the average charge state of Co keeps increasing from +1.25 to +1.33 (Fig. 5(b)), which is close to previously calculated results.[6,11] This reveals that both Co and O participate in the charge compensation during the delithiation process but for different stages. The charge compensation for delithiation is predominated by Co *via* changing Co^{3+} to Co^{4+} when less than 62.5% Li is removed and the charge compensation for delithiation is dominated by O at a high delithiation state through changing from O^{2-} to $(O_2)^{n-}$. Besides, the charge states of individual $O_{number\,30}$, $O_{number\,76}$, $Co_{number\,38}$, and $O_{number\,76}$ in Li_xCoO_2 are calculated (Fig. 5(a) and (b)), which show that there exists a slight difference between the average charge state and individual Co and O in Li_xCoO_2. The charge states of Co and O are almost linear with the delithiation state, while the charge states of individual Co and O change dramatically around 62.5% delithiation. This reveals that the charge compensation of Co and O in Li_xCoO_2 for delithiation is not uniform. A reasonable elemental doping, such as La and Al, can mitigate this non-uniformity and stabilize the crystalline structure of L_xCoO_2 at a high delithiation state.[4,44–47]

In addition, the change of O ↔ O interaction environments in the presence of CoO_6 slab migration during delithiation, which is correlated with the phase transformation of the Li_xCoO_2 structure. The phase transformation of Li_xCoO_2 directly influences the volume change of Li_xCoO_2. Fig. 6 demonstrates that the Co layer has a slight glide when 12.5% and 25% Li are extracted from $LiCoO_2$. The Co layer undergoes a huge displacement when the delithiation is more than 62.5%. The CoO_6 slab continues to glide, and the gradual angle, defined as the Co stacking in the $LiCoO_2$ along the 001 direction, decreases with further delithiation, which is consistent with recently reported *in situ* XRD and *ex situ* STEM.[48] This also indicates that the Li_xCoO_2 evolves from the O3 phase to the O1 phase, which also agrees well with reported observation.[48] More notably, this demonstrates that there is an accumulation of vacancy phenomenon, which is one of the main factors causing the phase transformation of $LiCoO_2$. The accumulation of Li vacancies becomes more severe with delithiation, accompanied by the rich-vacancy phase formation owing to the lower energy state. Therefore, this theoretically confirms that the CoO_6 slab glides continuously and is an intelligent dynamic response to the delithiation process, disclosing the existence of the accumulation of vacancy phenomenon in Li_xCoO_2 cathode materials during delithiation.

Conclusion

In this work, it reveals that the different delithiation paths have an impact on the initiation of volume shrinkage of Li_xCoO_2, which ranges between 62.5% and 75% delithiation. This means that the available capacity of the $LiCoO_2$ cathode is tunable by manipulating Li extraction sites and $LiCoO_2$ with poor reversible capacity can be improved *via* materials synthesis. In addition, the O ↔ O interlayer distance across the Li Layer ($O_{(d3)}$) mainly contributes to the volume increase when less than 62.5–75% removal of Li and the O ↔ O interlayer distance across the Co layer ($O_{(d2)}$) dominates the dramatic volume shrinkage of Li_xCoO_2 when delithiation is more than 62.5%. The ELF calculation shows that there is peroxo-like O ↔ O formation during delithiation, which is more reasonable than

the reported COOP analysis for only specific O–O bonding state. Furthermore, the oxygen oxidation and the dramatic volume change point of Li_xCoO_2 are correlated. The delithiation state of Li_xCoO_2 will influence oxygen oxidation, which will induce dramatic volume changes in Li_xCoO_2. The volume shrinkage of Li_xCoO_2 has an impact on the oxygen oxidation in return. Moreover, the volume shrinkage of Li_xCoO_2 stems from the oxygen charge compensation, and the charge compensation of Co and O in Li_xCoO_2 for delithiation is not uniform, which can be remitted by implementing a doping strategy. This provides new insight into the fundamental reason for the dramatic volume change of Li_xCoO_2 from the electronic and atomic levels. We propose that the antisite defects of $LiCoO_2$ should be designed carefully, which lead to weaker Co–O bond strength and further oxygen release, although they enable a higher intercalation potential of $LiCoO_2$. More importantly, $LiCoO_2$ material design with elemental doping, oxygen defects, Li defects, and Co defects contributes to the improvement of the reversible capacity of $LiCoO_2$.

Data availability

The Li_xCoO_2 structures at different delithiation states are provided in the ESI.† All structures used for simulations and other data supporting the findings of this work are available upon request.

Author contributions

Yufang He conducted the simulations and wrote the manuscript; Xiangming He and Li Wang provided guidance and suggestions for this work; Jonghyun Park and Hiep Pham provided suggestions and modified the manuscript; Bo Zhang and Hong Xu provided suggestions for the calculations and manuscript.

Conflicts of interest

The authors declare no competing interests.

Acknowledgements

This work was sponsored by the National Natural Science Foundation of China (No. U21A20170), the National Science and Technology Major Project (No. 2019YFE0100200) and China Postdoctoral Science Foundation (No. 2022M711791 and 2021M701873). We also appreciate the Joint Work Plan for Research Projects under the Clean Vehicles Consortium at U.S. and China – Clean Energy Research Center (CERC-CVC) and the Tsinghua University – Zhangjiagang Joint Institute for Hydrogen Energy and Lithium-Ion Battery Technology.

References

1 K. Mizushima, P. C. Jones, P. J. Wiseman and J. B. Goodenough, Li_xCoO_2 ($0 < x < -1$): A new cathode material for batteries of high energy density, *Mater. Res. Bull.*, 1980, **15**(6), 783–789.
2 Y. Chen, Y. Kang, Y. Zhao, L. Wang, J. Liu, Y. Li, Z. Liang, X. He, X. Li, N. Tavajohi and B. Li, A review of lithium-ion battery safety concerns: The issues, strategies, and testing standards, *J. Energy Chem.*, 2021, **59**, 83–99.
3 L. Wang, J. Ma, C. Wang, X. Yu, R. Liu, F. Jiang, X. Sun, A. Du, X. Zhou and G. Cui, A novel bifunctional self-stabilized strategy enabling 4.6 V $LiCoO_2$ with excellent long-term cyclability and high-rate capability, *Adv. Sci.*, 2019, **6**(12), 1900355.
4 Q. Liu, X. Su, D. Lei, Y. Qin, J. Wen, F. Guo, Y. A. Wu, Y. Rong, R. Kou, X. Xiao, F. Aguesse, J. Bareño, Y. Ren, W. Lu and Y. Li, Approaching the capacity limit of lithium cobalt oxide in lithium ion batteries *via* lanthanum and aluminium doping, *Nat. Energy*, 2018, **3**(11), 936–943.
5 P. Zhao, J. Yang, Y. Shang, L. Wang, M. Fang, J. Wang and X. He, Surface modification of polyolefin separators for lithium ion batteries to reduce thermal shrinkage without thickness increase, *J. Energy Chem.*, 2015, **21**(2), 138–144.
6 E. Hu, Q. Li, X. Wang, F. Meng, J. Liu, J. Zhang, K. Page, W. Xu, L. Gu, R. Xiao, H. Li, X. Huang, L. Chen, W. Yang, X. Yu and X.-Q. Yang, Oxygen-redox reactions in $LiCoO_2$ cathode without O–O bonding during charge-discharge, *Joule*, 2021, **5**(3), 720–736.
7 J. L. Tebbe, A. M. Holder and C. B. Musgrave, Mechanisms of $LiCoO_2$ Cathode Degradation by Reaction with HF and Protection by Thin Oxide Coatings, *ACS Appl. Mater. Interfaces*, 2015, **7**(43), 24265–24278.
8 A. Yano, M. Shikano, A. Ueda, H. Sakaebe and Z. Ogumi, $LiCoO_2$ degradation behavior in the high-voltage phase transition region and improved reversibility with surface coating, *J. Electrochem. Soc.*, 2017, **164**, A6116–A6122.
9 J. Qian, L. Liu, J. Yang, S. Li, X. Wang, H. L. Zhuang and Y. Lu, Electrochemical surface passivation of $LiCoO_2$ particles at ultrahigh voltage and its applications in lithium-based batteries, *Nat. Commun.*, 2018, **9**(1), 4918.
10 G. G. Amatucci, J. M. Tarascon and L. C. Klein, CoO_2, the end member of the Li_xCoO_2 solid solution, *J. Electrochem. Soc.*, 1996, **143**(3), 1114–1123.
11 A. Van der Ven, M. K. Aydinol, G. Ceder, G. Kresse and J. Hafner, First-principles investigation of phase stability in Li_xCoO_2, *Phys. Rev. B: Condens. Matter Mater. Phys.*, 1998, **58**(6), 2975–2987.
12 J. N. Reimers and J. R. Dahn, Electrochemical and *in situ* X-ray diffraction studies of lithium intercalation in Li_xCoO_2, *J. Electrochem. Soc.*, 1992, **139**(8), 2091–2097.
13 J. Barker, R. Pynenburg, R. Koksbang and M. Y. Saidi, An electrochemical investigation into the lithium insertion properties of Li_xCoO_2, *Electrochim. Acta*, 1996, **41**(15), 2481–2488.
14 T. Ohzuku and A. Ueda, Why transition metal (di) oxides are the most attractive materials for batteries, *Solid State Ionics*, 1994, **69**(3), 201–211.
15 E. McCalla, A. M. Abakumov, M. Saubanère, D. Foix, E. J. Berg, G. Rousse, M.-L. Doublet, D. Gonbeau,

P. Novák, G. Van Tendeloo, R. Dominko and J.-M. Tarascon, Visualization of O–O peroxo-like dimers in high-capacity layered oxides for Li-ion batteries, *Science*, 2015, **350**(6267), 1516–1521.

16 R. A. House, U. Maitra, M. A. Pérez-Osorio, J. G. Lozano, L. Jin, J. W. Somerville, L. C. Duda, A. Nag, A. Walters, K.-J. Zhou, M. R. Roberts and P. G. Bruce, Superstructure control of first-cycle voltage hysteresis in oxygen-redox cathodes, *Nature*, 2020, **577**(7791), 502–508.

17 M. Sathiya, G. Rousse, K. Ramesha, C. P. Laisa, H. Vezin, M. T. Sougrati, M. L. Doublet, D. Foix, D. Gonbeau, W. Walker, A. S. Prakash, M. Ben Hassine, L. Dupont and J. M. Tarascon, Reversible anionic redox chemistry in high-capacity layered-oxide electrodes, *Nat. Mater.*, 2013, **12**(9), 827–835.

18 D.-H. Seo, J. Lee, A. Urban, R. Malik, S. Kang and G. Ceder, The structural and chemical origin of the oxygen redox activity in layered and cation-disordered Li-excess cathode materials, *Nat. Chem.*, 2016, **8**(7), 692–697.

19 S. Li, Z. Liu, L. Yang, X. Shen, Q. Liu, Z. Hu, Q. Kong, J. Ma, J. Li, H. J. Lin, C. T. Chen, X. Wang, R. Yu, Z. Wang and L. Chen, Anionic redox reaction and structural evolution of Ni-rich layered oxide cathode material, *Nano Energy*, 2022, **98**, 107335.

20 H. Chen and M. S. Islam, Lithium extraction mechanism in Li-rich Li_2MnO_3 involving oxygen hole formation and dimerization, *Chem. Mater.*, 2016, **28**, 6656–6663.

21 J. Hafner and G. Kresse, The Vienna Ab-Initio Simulation Program VASP: An Efficient and Versatile Tool for Studying the Structural, Dynamic, and Electronic Properties of Materials, in *Properties of Complex Inorganic Solids*, ed. A. Gonis, A. Meike and P. E. A. Turchi, Springer, US, Boston, MA, 1997, pp.69–82.

22 J. P. Perdew, K. Burke and M. Ernzerhof, Generalized gradient approximation made simple, *Phys. Rev. Lett.*, 1996, **77**(18), 3865–3868.

23 G. Kresse and J. Furthmüller, Efficient iterative schemes for *ab initio* total-energy calculations using a plane-wave basis set, *Phys. Rev. B: Condens. Matter Mater. Phys.*, 1996, **54**(16), 11169–11186.

24 G. Kresse and J. Furthmüller, Efficiency of *ab initio* total energy calculations for metals and semiconductors using a plane-wave basis set, *Comput. Mater. Sci.*, 1996, **6**(1), 15–50.

25 J. M. Lim, T. Hwang, D. Kim, M. S. Park, K. Cho and M. Cho, Intrinsic origins of crack generation in Ni-rich $LiNi_{0.8}Co_{0.1}Mn_{0.1}O_2$ layered oxide cathode material, *Sci. Rep.*, 2017, **7**(1), 39669.

26 B. Zhang, Y. He, H. Gao, X. Wang, J. Liu, H. Xu, L. Wang and X. He, Unraveling the doping mechanisms in lithium iron phosphate, *Energy Mater.*, 2022, **2**(2), 200013.

27 B. Silvi and A. Savin, Classification of chemical bonds based on topological analysis of electron localization functions, *Nature*, 1994, **371**(6499), 683–686.

28 K. Momma and F. Izumi, VESTA 3 for three-dimensional visualization of crystal, volumetric and morphology data, *J. Appl. Crystallogr.*, 2011, **44**, 1272–1276.

29 Y. Kang, X. Guo, Z. Guo, J. Li, Y. Zhou, Z. Liang, C. Han, X. He, Y. Zhao, N. Tavajohi and B. Li, Phosphorus-doped lithium- and manganese-rich layered oxide cathode material for fast charging lithium-ion batteries, *J. Energy Chem.*, 2021, **62**, 538–545.

30 W. Tang, E. Sanville and G. Henkelman, A grid-based Bader analysis algorithm without lattice bias, *J. Phys.: Condens. Matter*, 2009, **21**(8), 084204.

31 E. Sanville, S. D. Kenny, R. Smith and G. Henkelman, Improved grid-based algorithm for Bader charge allocation, *J. Comput. Chem.*, 2007, **28**(5), 899–908.

32 G. Henkelman, A. Arnaldsson and H. Jónsson, A fast and robust algorithm for Bader decomposition of charge density, *Comput. Mater. Sci.*, 2006, **36**(3), 354–360.

33 M. Yu and D. R. Trinkle, Accurate and efficient algorithm for Bader charge integration, *J. Chem. Phys.*, 2011, **134**(6), 064111.

34 M. A. Rodriguez, D. Ingersoll and D. H. Doughty, *In situ* X-ray diffraction studies on lithium-ion battery cathodes, *MRS Online Proc. Libr.*, 1999, **575**(1), 65–70.

35 W. Hu, Y. Chen, H. Kou, Y. Wang, H. Wan and H. Li, First-principles study on the electronic structure of $LiCoO_2$ with intrinsic defects, *Ionics*, 2022, **28**(7), 3139–3143.

36 C. Liu, Z. G. Neale and G. Cao, Understanding electrochemical potentials of cathode materials in rechargeable batteries, *Mater. Today*, 2016, **19**(2), 109–123.

37 E. Antolini, $LiCoO_2$: Formation, structure, lithium and oxygen nonstoichiometry, electrochemical behaviour and transport properties, *Solid State Ionics*, 2004, **170**(3), 159–171.

38 Y. Lyu, X. Wu, K. Wang, Z. Feng, T. Cheng, Y. Liu, M. Wang, R. Chen, L. Xu, J. Zhou, Y. Lu and B. Guo, An overview on the advances of $LiCoO_2$ cathodes for lithium-ion batteries, *Adv. Energy Mater.*, 2021, **11**(2), 2000982.

39 C. Zheng, Z. Yang, J. Feng, J. Zhong, Z. Wei and J. Li, Bifunctional surface modification coupled with oxygen defect engineering enables high performance Li-rich cathodes, *J. Mater. Chem. A*, 2022, **10**(30), 16046–16060.

40 J. N. Reimers, J. R. Dahn and U. G. V. Sacken, Effects of impurities on the electrochemical properties of $LiCoO_2$, *J. Electrochem. Soc.*, 1993, **140**, 2752–2754.

41 J. M. Tarascon, G. Vaughan, Y. Chabre, L. Seguin, M. Anne, P. Strobel and G. Amatucci, *In situ* structural and electrochemical study of $Ni_{1-x}Co_xO_2$ metastable oxides prepared by soft chemistry, *J. Solid State Chem.*, 1999, **147**(1), 410–420.

42 Y. Shao-Horn, L. Croguennec, C. Delmas, E. C. Nelson and M. A. O'Keefe, Atomic resolution of lithium ions in $LiCoO_2$, *Nat. Mater.*, 2003, **2**(7), 464–467.

43 P. Fuentealba; E. Chamorro and J. C. Santos, Chapter 5 Understanding and using the electron localization function, in *Theoretical and Computational Chemistry*, ed. A. Toro-Labbé, Elsevier, 2007, pp.57–85, vol. 19.

44 J. N. Zhang, Q. Li, C. Ouyang, X. Yu, M. Ge, X. Huang, E. Hu, C. Ma, S. Li, R. Xiao, W. Yang, Y. Chu, Y. Liu, H. Yu, X. Q. Yang, X. Huang, L. Chen and H. Li, Trace doping of multiple elements enables stable battery cycling of $LiCoO_2$ at 4.6 V, *Nat. Energy*, 2019, **4**(7), 594–603.

45 S. T. Myung, N. Kumagai, S. Komaba and H. T. Chung, Effects of Al doping on the microstructure of $LiCoO_2$ cathode materials, *Solid State Ionics*, 2001, **139**(1), 47–56.

46 F. E. Er-Rami, M. Duffiet, S. Hinkle, J. Auvergniot, M. Blangero, P. E. Cabelguen, K. Song, F. Weill, C. Delmas and D. Carlier, Understanding the role of Al doping of $LiCoO_2$ on the mechanisms upon cycling up to high voltages ($\geq$4.6 V *vs.* Li^+/Li), *Chem. Mater.*, 2022, **34**(10), 4384–4393.

47 S. Song, Y. Li, K. Yang, Z. Chen, J. Liu, R. Qi, Z. Li, C. Zuo, W. Zhao, N. Yang, M. Zhang and F. Pan, Interplay between multiple doping elements in high-voltage $LiCoO_2$, *J. Mater. Chem. A*, 2021, **9**(9), 5702–5710.

48 S. Li, Y. Sun, A. Gao, Q. Zhang, X. Lu and X. Lu, Sustainable $LiCoO_2$ by collective glide of CoO_6 slabs upon charge/discharge, *Proc. Natl. Acad. Sci. U. S. A.*, 2022, **119**(20), e2120060119.